11th International Symposium on Turbulence and Shear Flow Phenomena (TSFP11)
Southampton, UK, July 30 to August 2, 2019

Aerodynamic Load Control on a 3-D Wing using Distributed Bleed

Daniel J. Heathcote
Department of Mechanical Engineering
Georgia Institute of Technology
771 Ferst Drive, Atlanta, GA, 30332, USA
Daniel.Heathcote@me.gatech.edu

Michael DeSalvo
Department of Mechanical Engineering
Georgia Institute of Technology
771 Ferst Drive, Atlanta, GA, 30332, USA
Michael.DeSalvo@me.gatech.edu

Ari Glezer
Department of Mechanical Engineering
Georgia Institute of Technology
771 Ferst Drive, Atlanta, GA, 30332, USA
Ari.Glezer@me.gatech.edu

ABSTRACT

The fundamental characteristics of aero-effected flight control using distributed bleed are investigated in wind tunnel experiments using a 3-D wing model. Aerodynamic control is achieved by large-area air bleed through the aerodynamic surfaces that is driven by inherent pressure differences in flight (e.g., between and across the pressure and suction surfaces of the wing). The interaction between the bleed (effectively distributions of surface "sinks" and "sources") and the cross flow leverages the generation and regulation of vorticity concentrations on or near the surface to locally alter its apparent aerodynamic shape and therefore the distributions of aerodynamic forces and moments without mechanically moving control surfaces. The present investigations explore the efficacy of passive bleed configurations for direct lift control and demonstrate lift decrements or increments of up to -28% or +11% with virtually no penalty in drag. Stereo PIV measurements indicate a significant reduction in the streamwise circulation distribution in the presence of bleed, reducing lift.

INTRODUCTION

Passive porosity using surface slots or perforations with the objective of altering the pressure distributions for flow control over aerodynamic surfaces has been investigated since the 1920s (Lachmann, 1924, Weick and Shortal, 1933). Over the years, it has shown promise for a number of applications including mitigation of shock waves on transonic airfoils (Savu and Trifu, 1984), reduction of base drag on bluff bodies (Tanner, 1975), and control of flow separation (Kraushaar and Chokani, 1997). Bauer and Hemsch (1994) explored these effects for alleviating asymmetries in aerodynamic forces on a tangent-ogive forebody using patches of porosity on the surface to drive flow between high- and low-pressure domains and reported reduced variations in normal and yaw force coefficients. In a numerical investigation, Hunter et al. (2001) demonstrated passive porosity control over the nose and wing surfaces of a generic tailless aircraft for generating variations in the longitudinal pitching moment and yaw force. A few studies of aerodynamic bleed attempted to actively regulate the interactions between the bleed and the cross flow. For example, Patel et al. (2003) showed that regulation of bleed through fins of an axisymmetric munition model using microvalve arrays can be used for steering.

Kearney and Glezer (2011, 2012) used distributed active bleed to manipulate the surface vorticity layer near the leading edge of a 2-D airfoil and thereby control the flow about the airfoil and the aerodynamic loads at pre-and post-stall angles of attack. Quasi-steady and time-periodic regulation of the bleed flow allowed for continuous deflection of the surface vorticity layer towards or away from the suction surface, leading to an alteration of the aerodynamic shape and resulting in significant variation of lift and pitching moment relative to the base flow.

The present investigation extends the earlier work to a 3-D aircraft wing where the bleed is applied at several spanwise locations. The effects of the bleed on the global aerodynamic loads and their spanwise distribution as well as on the flow field in the near-wake are invested at pre-stall angles of attack over a range of flap angles.

EXPERIMENTAL METHODOLOGY

The present wind tunnel investigations of application of distributed bleed utilize a 3-D semi-span wing model based upon NASA's HARV F/A-18. As shown in Fig. 1(a), the model incorporates a leading edge extension (LEX) and a plain flap, covering the final 30% local chord. The model has a mean chord length, $\bar{c} = 0.39$ m, excluding the LEX and a span, $b = 0.62$ m. The wind tunnel's square test section measures 0.91 x 0.91 m, and the test are performed at a free-stream speed, $U_0 = 30$ m/s or $Re_c = 7.6 \cdot 10^5$. The model is mounted vertically in the wind tunnel, supported from below by a hollow bar attached to a load cell and stepper motor assembly. This allows for control of the model's angle of attack, α ($0 < \alpha < 16°$) while measuring all six components of aerodynamic forces and moments. In addition, the plain flap incorporates a mechanism for varying the flap angle, δ between 0 and 42° (in the presented results, $\delta = 24$ and 42°). The wing is constructed of a series of rapid-prototyped, removable skin panels mounted over an aluminium structure. The skin panels are interchangeable, allowing for several bleed configurations on the pressure and suction surfaces at the root, mid-span and tip having open areas of 4.3%, 4.5% and 3.4% of the wing reference area, respectively (cf., Fig 1(a), with the colours corresponding to those used in the later figures). Each

bleed panels consist of a series of slots (Fig 1(b)) that enable unhindered air flow through the internal wing volume.

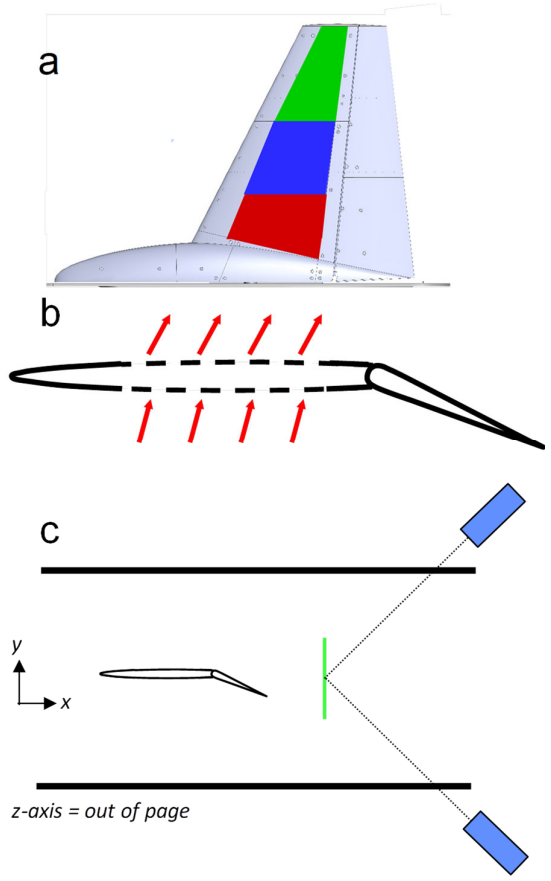

Figure 1. (a) Planform of wind tunnel model, colours indicate bleed panel locations (b) Schematic of distributed bleed configuration. (c) Top view of stereoscopic PIV camera and laser arrangement in wake of wind tunnel model.

The flow in the near wake of the wing is characterized in a cross-stream plane normal to the free stream along the span ($z/b = 1.2$ from 0.1) using stereoscopic PIV as shown schematically in Fig. 1(c). Composite time-averaged velocity, streamwise vorticity, and turbulent stresses are computed within ten partially-overlapping windows within this plane to characterise the full wake. The flow is seeded using micron-scale smoke particles and is illuminated using a double-pulsed Nd-YAG laser. Image pairs were captured using a pair of 1600 x 1200 pixel CCD cameras, placed downstream of the image plane. The measurements are ensemble-averaged from 1000 instantaneous vector fields.

RESULTS

Aerodynamic Force Measurements

Aerodynamic load measurements were also conducted using bleed at varying spanwise locations, to assess their effects on lift (C_L), drag, (C_D), pitching ($C_{M1/4}$) and rolling moments (C_R). Figures 2 and 3 show results considering two flap angles, $\delta = 24°$ and 42°. Further force measurements are presented in DeSalvo et al. 2019. The increments in aerodynamic loads (relative to the baseline airfoil) are presented, along with the baseline value for reference.

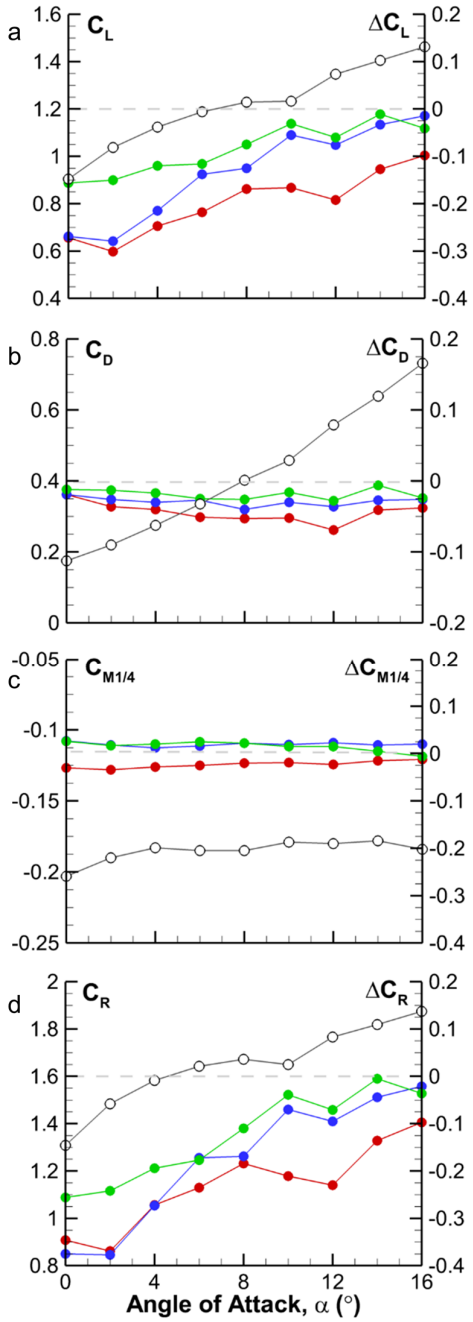

Figure 2: Variation of (a) ΔC_L, (b) ΔC_D, (c) ΔC_M, and (d) ΔC_R with α relative to baseline for airfoil with $\delta = 24°$ and aerodynamic bleed from mid-chord at the root (●), mid-span (●) and tip (●). Baseline values (○) shown for reference.

Considering $\delta = 24°$ flap deflection (Fig. 2), the lift loss (Fig. 2(a)) is greatest in the presence of bleed at the root, varying from $\Delta C_L = -0.30$ at $\alpha = 2°$ (30% of baseline) to $\Delta C_L = -0.10$ at $\alpha = 16°$ (7% of baseline). Bleed from the tip panel (with open area 80% of the root bleed panel) leads to approximately half as much lift loss. This may be due to the reduced lift per unit span near the tip in the presence of the tip vortex (described later) and shorter local chord. For $\alpha \leq 4°$, bleed at mid-span leads to lift reduction nearly as large as bleed at the root. Meanwhile, for α

≥ 10º the lift reduction for mid-span bleed is reduced to a level comparable to tip bleed. Reductions in lift are accompanied by reduced drag (Fig. 2(b)) which is largest in the presence of root bleed (having the greatest lift loss). The drag reduction is nominally commensurate with the lift loss, suggesting a reduction in lift-induced drag. Since the bleed slots are predominantly located near or downstream of the mean quarter-chord, reduction in lift at the bleed slots leads to a small nose-up change in pitching moment, $\Delta C_M = +0.02$ (Fig. 2(c)) for $\alpha \leq 12º$. For $\alpha \geq 14º$, the pitching moment is nose-down ($\Delta C_M \approx -0.02$) in the presence of root and tip bleed, while lift is reduced (Fig. 2(a)). The change in C_R (Fig. 2(d)) is largest with root bleed, while bleed placed close to the tip leads to approximately 70% of ΔC_R with root bleed while ΔC_L is ~50% as large (cf. Fig. 2(a)), because of the increased moment arm at the tip. As with ΔC_L, ΔC_R with mid-span bleed falls between the levels of root and tip bleed.

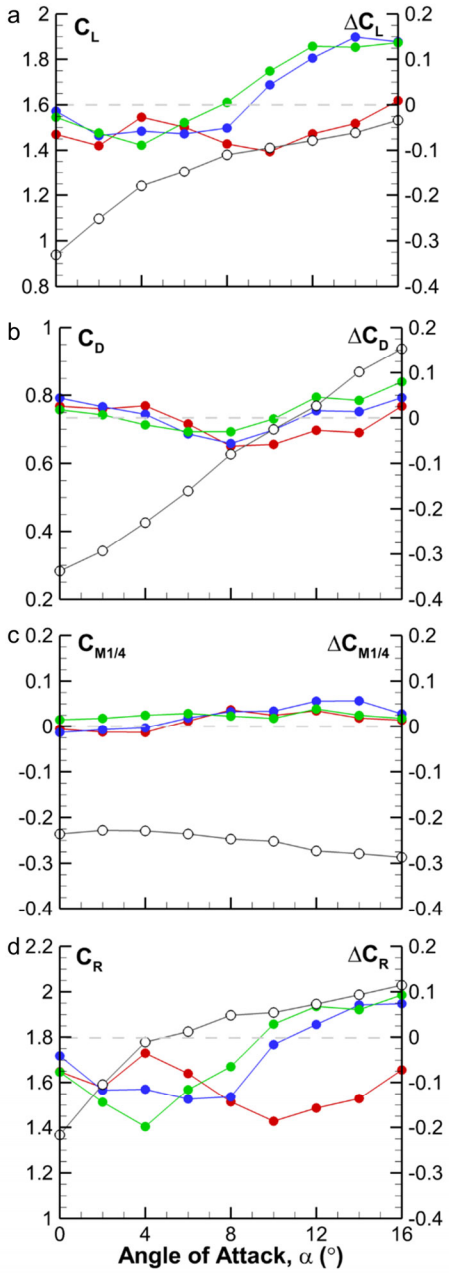

Figure 3: Variation of (a) ΔC_L, (b) ΔC_D, (c) ΔC_M, and (d) ΔC_R with α relative to baseline for airfoil with δ = 42° and aerodynamic bleed from mid-chord at the root (●), mid-span (●) and tip (●). Baseline values (○) shown for reference.

The effects of bleed on aerodynamic loads for δ = 42º are shown in Fig. 3. The change in lift (Fig. 3(a)) for root bleed is negative (on the order of $\Delta C_L = -0.1$), significantly reduced compared to δ = 24º. However, for $\alpha \geq 10º$, lift is increased in the presence of mid-span and tip bleed by as much as $\Delta C_L = +0.15$. It is hypothesized that bleed flow exiting through downstream-oriented slots on the suction surface into the boundary layer mitigates separation over the flap, resulting in an increased extent in flow attachment and hence higher lift. The reduction in drag (Fig. 3(b)) with root bleed is nominally proportional to the reduction in lift, suggesting lift-induced drag is reduced. In the presence of mid-span and tip bleed for $\alpha \geq 8º$, there is a net increase in drag on the order of $\Delta C_D = +0.04$ because of the increased lift. Changes in pitching moment (Fig. 3(c)) are in the nose-up direction on the order of $\Delta C_M = +0.03$ because of lift loss downstream of the mean quarter-chord. Changes in rolling moment (Fig. 3(d)) follow similar trends to the changes in lift, with changes due to the tip bleed having larger magnitude because of increased moment arm.

Flow Field Measurements

Figures 4 and 5 present ensemble or time-averaged flow field measurements in the wake of the wing, 0.33c downstream of the wing trailing edge for baseline and bleed cases of interest selected from the aerodynamic load measurements. Flow field measurements are presented for α = 2° and flap angle, δ = 24°, for which the maximum reduction in lift occurs ($\Delta C_L = -0.30$ with bleed at the root). Further flow field measurements considering the effect of angle of attack can be seen in DeSalvo et al. 2019. The bleed panel location examined in each of the figures is indicated by the black, dashed lines.

The effect on streamwise velocity and vorticity at α = 2° in the presence of bleed is indicated in Fig. 4. The baseline streamwise velocity data (Fig. 4(a)) indicates a substantial reduction in its magnitude in the wake of the wing. The wake is deflected to the left, beyond the pressure surface, due to the presence of the flap, inducing significant downwash (cf. Fig 4(e)). A reduction in streamwise velocity at the wing tip (z/S = 1) indicates the presence of the tip vortex. In board, the velocity deficit is larger than that near the root, indicating that the wing may be prone to separation close to the wing tip.

For all cases considering bleed, the deficit in streamwise component is increased about the bleed panel location, but to varying degrees. Bleed placed near the root and mid-span (Figs. 4(b) and (c)) produces a large velocity deficit, with the streamwise velocity in this region is indicating that the flow is separated over the flap. However, Figure 4(d) indicates that the flow velocity deficit within the wing tip vortex is increased in magnitude (from 0.60 to 0.58), when compared to the baseline. Near the bleed panel, the area over which the velocity deficit is observable is increased when compared to the baseline condition.

Figures 4 (e) to (h) present the streamwise vorticity component. For bleed placed close to the mid-span and root, regions of positive (anticlockwise) and negative (clockwise) vorticity are observed, for example in Fig. 4(f) at z/S = 0.55 and 0.3 respectively for the mid-span location. These indicate the interaction between the primarily streamwise flow over the wing and cross-stream flow through the bleed panel in a similar

manner to the interaction between a fluidic vortex generator or synthetic jet and cross-flow (e.g. Hansen & Bons. 2006, Van Buren et al. 2014). Between the two vortices, downwash is reduced in comparison to the baseline wing as an effect of the cross-stream bleed flow. This effect is similar to that of Kearney & Glezer (2012), displacing the flow away from the wing suction surface. The bleed flow's influence is also present beyond the bleed panel's spanwise extent. Towards the wing tip, a reduction in anticlockwise vorticity is noted between $0.6 < z/S < 0.8$ (Fig. 4(f)). Inboard of the bleed panel, anticlockwise vorticity is increased in comparison to the baseline configuration, coupled to increased downwash.

Bleed near the root creates the largest change in lift ($\Delta C_L = -0.30$; cf. Figure 2), while bleed near the tip yields a smaller lift reduction ($\Delta C_L = -0.16$) than at mid-span. As with bleed from the mid-span location, bleed near the root (Fig. 4(e) creates similar regions of opposing vorticity towards the edges of the bleed panel. However, the region of positive, clockwise vorticity is of increased strength. In the presence of bleed, the cross-stream velocity component changes from downwash (for the baseline wing) to upwash in the vicinity of the bleed panel. Outboard of the bleed panel, however, an increase in downwash suggests increased lift generation. Considering the tip vortex circulation, bleed placed at the root reduces the normalised circulation by 12% to 0.25, from the baseline value of 0.28. This suggests that bleed from the inboard portion of the wing significantly affects the flow over the outer span and influences the distribution of lift across the entire wing span.

The effects of bleed near the wing tip are indicated in Fig. 4(h). The streamwise vorticity distribution in the wake is like the baseline configuration (Fig. 4(e)), but with several key differences. No discrete region of positive vorticity is generated outboard of the bleed panel near the tip, unlike that produced by the other configurations. Instead, the changes in streamwise vorticity at the bleed panel's outboard extent manifest in the form of a reduction in the tip vortex circulation. Bleed near the wing tip reduces circulation by 19% to 0.22. The inboard extent of the bleed panel is indicated by a domain of increased negative vorticity near $z/S = 0.7$. As with bleed at mid-span and near the root, a reduction in downwash is present across the extent of the bleed panel near the tip, indicating a reduction in lift production across the bleed panel. However, the influence of bleed near the tip is minimal inboard of the panel location.

To further elucidate the effects of bleed on the flow, the normalized streamwise ($\overline{u'u'}/U_0^2$) and in-plane ($\overline{v'w'}/U_0^2$) turbulent stresses were extracted from the PIV measurements and are presented in Figs. 5(a) to (d) and (e) to (h), respectively. The streamwise stress in the base flow (Fig 5(a)) is most pronounced downstream of the outboard section of the wing and intensifies towards the wing tip, and becomes concentrated within the core of the tip vortex ($z/S = 1$). However, the presence of bleed at the at the root and mid-span sections (Figs. 5(b) and (c)), leads to reduction in ($\overline{u'u'}/U_0^2$) near the tip along with a concomitant precipitous increase about the bleed segments. It is noteworthy that the reduction in streamwise stresses near the tip section is also manifested within the core of the tip vortex which appears to weaken in the presence of bleed (cf. Figs. 4(g) and (f)). In the presence of bleed, the measurements exhibit clear spanwise maxima along the suction and pressure surfaces of the wing, which are indicative of two separated shear layers that bound the deficit in the streamwise velocity shown in Figs. 4(b) and (c) where $\overline{u'u'}/U_0^2$ has a clear minimum near the cross-stream center of the wake. It appears that the bleed-induced reduction in $\overline{u'u'}/U_0^2$ towards the wing tip is associated with the reduction in spanwise velocity towards the tip. As the bleed is migrated towards the tip section $\overline{u'u'}/U_0^2$ intensifies there (Fig. 5(d)) along with the increase in the velocity deficit

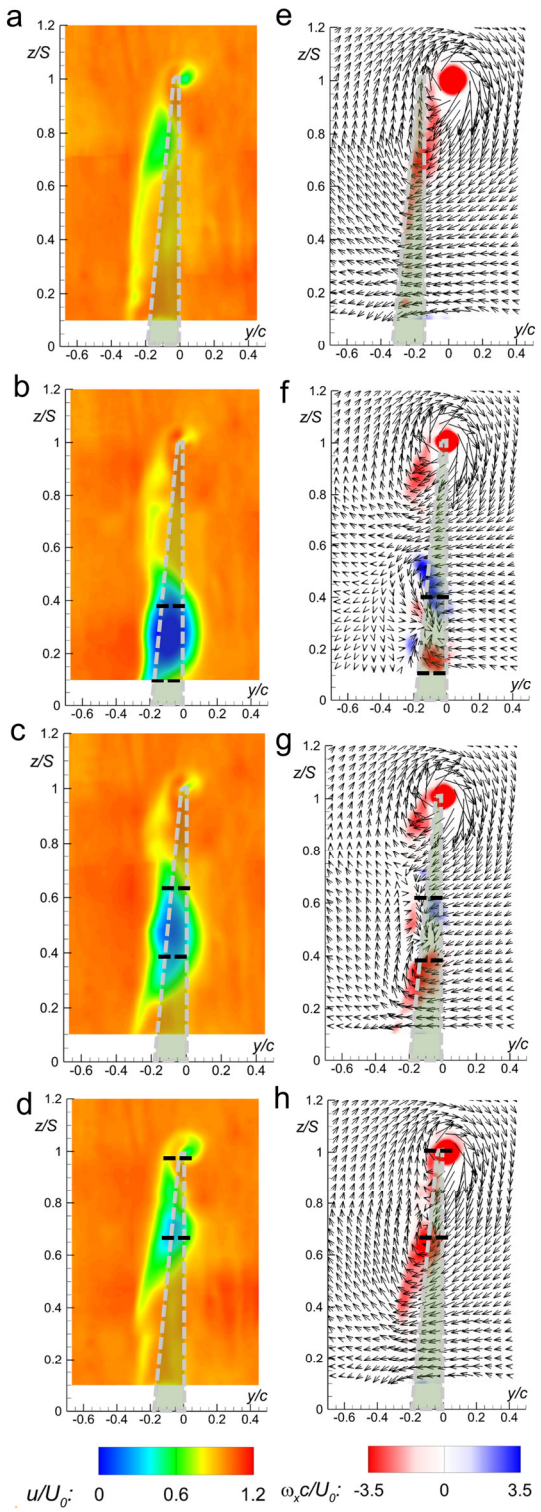

Figure 4. Comparison of time-averaged normalized streamwise velocity ($\overline{u}/U_0$) and vorticity ($\omega_x\bar{c}/U_0$) with in-plane velocities ($\overline{v}/U_0$ and $\overline{w}/U_0$) for $\alpha = 2°$. Baseline (a & e), bleed at the root (b & f) , mid-span (c & g) and wingtip (d & h).

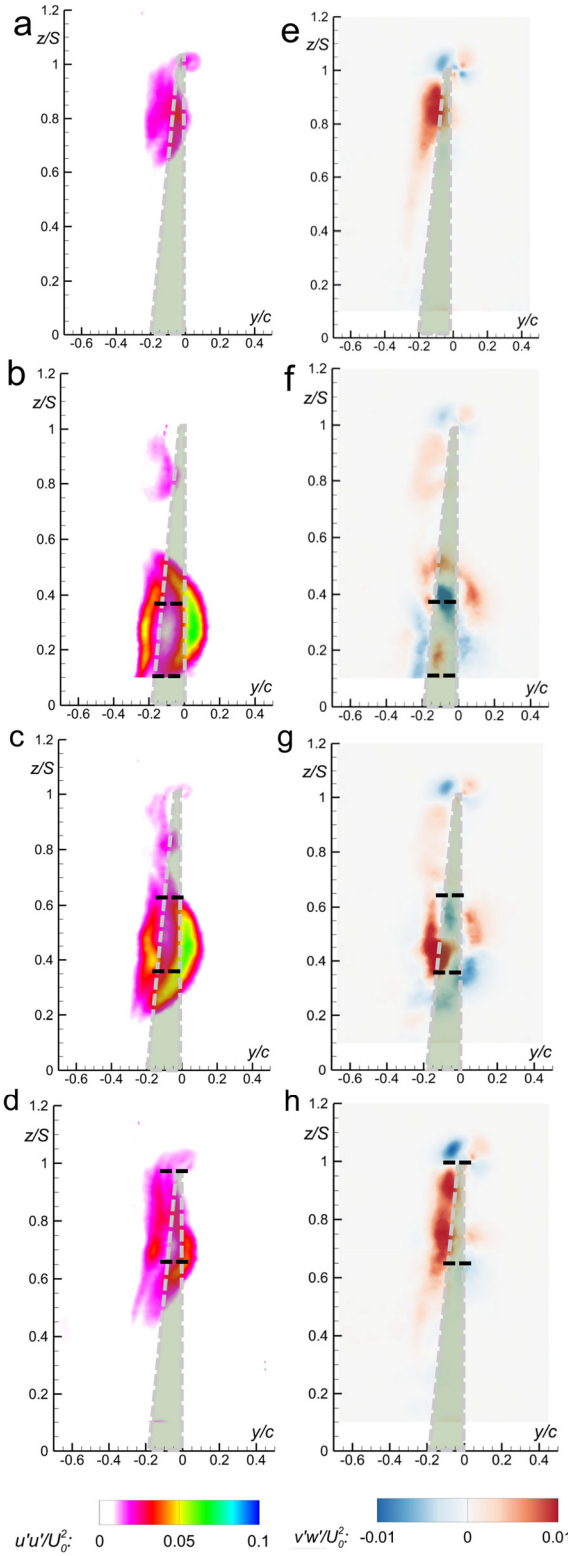

Figure 5. Comparison of time-averaged streamwise ($u'u'/U_0^2$) and in-plane ($v'w'/U_0^2$) turbulent stresses for $\alpha = 2°$. Baseline (a & e), bleed at the root (b & f) , mid-span (c & g) and wingtip (d & h).

compared to the base flow (cf. Figs. 4(d) and (a)), and the there is also an increase in the streamwise stress within the core of the vortex.

Figures 5(e) to (h) show the in-plane turbulent shear stress, $v'w'/U_0^2$. In the base flow (Fig. 5(e)), $v'w'/U_0^2$ is higher within the deflected wing wake near the tip and is mostly positive indicating that the sense of each velocity component is positive. At the wing tip within the tip vortex there are two cross pairs of $v'w'/U_0^2$ of opposite sense commensurate with the rotation within the core of the vortex. These regions indicate the presence and meandering of the tip vortex.

The presence of bleed within the segment close to the wing root (Fig. 5(f)) leads to a clear increase in $v'w'/U_0^2$ around the bleed panel. Moreover, the fluctuations of opposite sense present at either spanwise end of the bleed panel indicate the presence of the counter-rotating streamwise vortex pairs at each end as indicated by the vorticity concentrations in Figs. 4(f) and (g). Each of the vortex pairs is associated with streamwise vorticity that originates from the counter-rotating sense of spanwise concentrations on the suction and pressure surfaces. Similar effects are observed for the mid-span bleed in Fig. 5(f). Bleed at the tip segment does not seem to lead to the formation of opposite sense edge vortex pairs but still indicates two (positive) spanwise concentrations with maxima near each edge of the bleed segment on the suction side. It is noteworthy that the reduction in the strength of the tip vortex in Fig. 4(h) is accompanied by intensification of $v'w'/U_0^2$. The increased fluctuations indicate that the bleed flow interacts to disrupt the vortical flow.

Spanwise Distribution of Circulation

While the PIV measurements in Figs. 4 and 5 qualitatively show the effects of employing bleed at different spanwise locations, it is important to consider the quantitative effects on the lift distribution. The effect of bleed can be assessed from quantities derived from the sPIV measurements such as circulation per unit span, from which the change in lift distribution provided by bleed can be derived. The streamwise circulation is calculated from the streamwise vorticity in the wake by integrating in the spanwise (z-) and cross-stream (y-) directions:

$$\Gamma_x = \int_0^S \int_{y_{min}}^{y_{max}} \omega_x(y,z)\, dy\, dz$$

Using Prandtl's lifting line theorem (Prandtl, 1923), the distribution of circulation can be estimated. From this, the variation in the lift distribution can be inferred. Prandtl's lifting line theorem considers a finite number of horseshoe vortices (schematically illustrated in Fig. 6), each consisting of a free-trailing component (streamwise vorticity shed into the wake, measured by the sPIV), and a bound component (spanwise vorticity along the lifting line which directly generates circulation, and thus lift) which are equal in magnitude. The change in circulation in one spanwise (z-) plane $\delta\Gamma_x(z)$ can be measured from the line integral of the streamwise vorticity and summed in the spanwise (z-) direction starting outboard of the wing tip to obtain the spanwise cumulative circulation distribution.

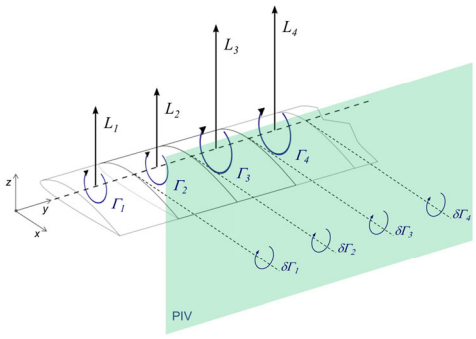

Figure 6. Illustration of Prandtl's lifting line theorem, indicating the circulation distribution of the wing.

The cumulative circulation $\Gamma_x(z)$ is shown in Fig. 7 for all three bleed configurations and the baseline configuration as a function of the normalized spanwise location, z/S. For the baseline wing at $\alpha = 2°$, the tip vortex provides a large increase in $\Gamma_x(z)$, accounting for circa 2/3 of the total circulation. Moving inboard from the tip, a gradual increase in $\Gamma_x(z)$ indicates that progressively increasing amounts of lift are generated toward the root. As the wing is tapered, the chord decreases significantly toward the wing tip, hence the lift per unit span, and local circulation, is reduced.

In the presence of bleed, the cumulative circulation decreases with the greatest reduction at the spanwise location of the bleed panel. With bleed at the tip, the contribution to cumulative circulation from the tip vortex is reduced, indicating a reduction in the tip vortex strength, described previously. Bleed from the root and mid-span has less effect on the tip vortex strength.

At any given spanwise location, the slope of the cumulative circulation represents the local contribution to lift. Beyond z/S = 0.6, the local contributions to lift for the baseline wing and in the presence of root bleed are comparable. In the presence of bleed near mid-span and the tip, the spanwise variation of $\Gamma_x(z)$ shows evidence of reduced lift in this region, as also indicated by a reduction in downwash (cf. Fig. 5). Inboard of the bleed panel (at all three locations), an increased $\Gamma_x(z)$ slope indicates an increased lift produced by the secondary vortical flow at the inner edge of the bleed panel (cf. Figure 5(f) to (h)).

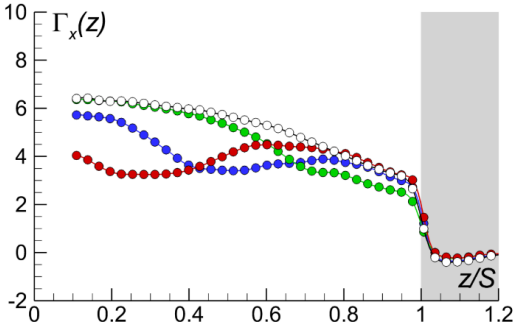

Figure 7. Spanwise variation of circulation for $\alpha = 2°$ and flap angle $\delta = 24°$ with aerodynamic bleed from mid-chord at the root (●), mid-span (●) and tip (●). Baseline values (○)

Within the bleed panel's spanwise extent, $\Gamma_x(z)$ is reduced. It is noteworthy that the in the presence of bleed at mid-span, circulation is influenced both inboard and outboard of the bleed panel. Due to the tapered wing planform, a higher proportion of lift is generated by the inboard sections. Therefore, it is suggested due to the inherent left distribution of the wing, bleed near the root leads to a greater reduction in circulation than bleed near the tip, and thus has a greater influence on the lift reduction.

CONCLUSIONS

Aerodynamic load and stereo PIV measurements have demonstrated the efficacy of distributed bleed actuation to control aerodynamic loads on a representative, three-dimensional wind tunnel wing model. Stereo-PIV measurements were used to quantify the effect of bleed from different spanwise locations on the wing's lift distribution. These data show that the bleed actuation induces significant alterations to the local flow field across the entire wing span. Circulation and sectional lift measurements suggest that bleed from the root and mid-span is more effective in reducing the lift owing to the inherently-higher lift toward the root of the base wing. The interaction of the bleed with the flow over the wing leads to a significant reduction in downwash, commensurate with a reduction in lift, and bleed at the wing tip significantly reduces the strength of the tip vortex. Direct aerodynamic load measurements show that the use of bleed near the mid-span of the wing (4% open area) reduces lift by as much as $\Delta C_L = -0.28$. Significant changes in lift were also measured using bleed near the root and tip, with the root section bleed increasing the lift reduction ($\Delta C_L = -0.30$) and less lift reduction with bleed from the tip ($\Delta C_L = -0.19$). In addition, certain bleed configurations at higher angles of attack ($\alpha \geq 10°$) yielded an increase in lift of up to 11%.

ACKNOWLEDGEMENTS

This project has been supported by the Office of Naval Research, monitored by Dr. Brian Holm-Hansen.

REFERENCES

Bauer, S., and Hemsch, M. "Alleviation of Side Force on Tangent-Ogive Forebodies using Passive Porosity," *Journal of Aircraft* Vol. 31, No. 2, 1992, pp. 354-361.

DeSalvo, M., Heathcote, D. J., Smith, M. J., and Glezer, A., "Direct Lift Control using Distributed Aerodynamic Bleed," *AIAA Scitech 2019 Forum,* AIAA-2019-0591, 2019

Hansen, L., Bons, J., "Flow Measurements of Vortex Generator Jets in Separating Boundary Layer", *Journal of Propulsion and Power,* Vol. 22, No. 3, 2006, pp. 558-566

Hunter, C., Viken, S., Wood, R., and Bauer, S., "Advanced Aerodynamic Design of Passive Porosity Control Effectors," *39th Aerospace Sciences Meeting and Exhibit*, AIAA-2001-0249, 2001

Kearney, J. M., and Glezer, A., "Aero-Effected Flight Control Using Distributed Active Bleed," *41st AIAA Fluid Dynamics Conference and Exhibit*, AIAA-2011-3099, 2011

Kearney, J. M., and Glezer, A., "Aerodynamic Control Using Distributed Bleed," *6th AIAA Flow Control Conference*, AIAA-2012-3246, 2012

Kraushaar, S., Chokani, N., "Afterbody Separation Control using Passive Porosity," *33rd Joint Propulsion Conference and Exhibit*, AIAA-1997-3003, 1997

Lachmann, G., "Results of Experiments with Slotted Wings." NACA Technical Memorandum No. 282, 1924

Tanner, M. "Reduction of Base Drag," *Progress in Aerospace Sciences* Vol. 16, No. 4, 1975, pp. 369-384.

Prandtl, L., "Applications of Modern Hydrodynamics to Aeronautics," NACA Report No. 116, June 1923.

Savu, G., and Trifu, O. "Porous Airfoils in Transonic Flow," *AIAA Journal* Vol. 22, No. 7, 1984, pp. 989-991.

Van Buren, T., Whalen, E., Amitay, M., "Vortex Formation of a finite-span synthetic jet: High Reynolds numbers", *Physics of Fluids*, Vol. 26, No. 014101, 2014, pp. 1- 22.

Weick, F. E., and Shortal, J. A., "The Effect of Multiple Fixed Slots and a Trailing-Edge Flap on the Lift and Drag of a Clark Y Airfoil." NACA Technical Report No. 427, 1933.